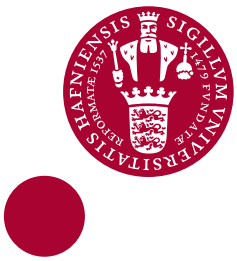

Purification, crystal structure determination and functional characterization of type III antifreeze proteins from the European eelpout Zoarces viviparus

Wilkens, Casper; Poulsen, Jens-Christian Navarro; Ramløv, Hans; Lo Leggio, Leila

Published in:
Cryobiology

DOI:
10.1016/j.cryobiol.2014.07.003

Publication date:
2014

Document version
Early version, also known as pre-print

Purification, crystal structure determination and functional characterization of type III antifreeze proteins from the European eelpout *Zoarces viviparus*

Casper Wilkens[a,c], Jens-Christian N. Poulsen,[a] Hans Ramløv[b] and Leila Lo Leggio[a1]

[a] Department of Chemistry, University of Copenhagen, Universitetsparken 5, DK-2100 Copenhagen, Denmark.

[b] Department of Science, Systems and Models, Universitetsvej 1, Roskilde University, DK-4000, Roskilde, Denmark

[c] current address: DTU Systems Biology, Technical University of Denmark, Soltofts Plads 224, DK-2800, Kgs. Lyngby, Denmark

[1] Corresponding author: Leila Lo Leggio: Department of Chemistry, University of Copenhagen, Universitetsparken 5, DK-2100 Copenhagen, Denmark. Tel: +45 35320295. Fax: +45 35320322. E-mail: leila@chem.ku.dk.

E-mails: Casper Wilkens, cwil@bio.dtu.dk; Hans Ramløv, hr@ruc.dk; Jens-Christian N. Poulsen, jnp@chem.ku.dk

Abstract

Antifreeze proteins (AFPs) are essential components of many organisms adaptation to cold temperatures. Fish type III AFPs are divided into two groups, SP isoforms being much less active than QAE1 isoforms. Two type III AFPs from *Zoarces viviparus*, a QAE1 (ZvAFP13) and an SP (ZvAFP6) isoform, are here characterized and their crystal structures determined. We conclude that the higher activity of the QAE1 isoforms cannot be attributed to single

residues, but rather a combination of structural effects. Furthermore both ZvAFP6 and ZvAFP13 crystal structures have water molecules around T18 equivalent to the tetrahedral-like waters previously identified in a neutron crystal structure. Interestingly, ZvAFP6 forms dimers in the crystal, with a significant dimer interface. The presence of ZvAFP6 dimers was confirmed in solution by native electrophoresis and gel filtration. To our knowledge this is the first report of dimerization of AFP type III proteins.

Keywords: Antifreeze protein, *Zoarces viviparus*, crystal structure, dimerization, protein purification

Abbreviations: TH (thermal hysteresis), T_{hf} (hysteresis freezing point), T_m (melting point), T_f (freezing point), AFP (antifreeze protein), IBS (ice binding site)

1. Introduction

Ectothermic animals that are frequently exposed to temperatures below the melting point (T_m) of their body fluids must either avoid freezing of their body fluids and survive the low temperatures or be able to tolerate ice formation in their tissues [22]. The body fluids of fish living in ice laden waters have a temperature similar to that of the surrounding water. The T_m of the body fluids is higher than that of the sea water, hence the fish are supercooled, and should in principle freeze when they ingest or touch an ice crystal [9].

Antifreeze proteins (AFPs) are an essential component of the adaptations many of these animals have evolved to survive low temperatures [7,9]. AFPs inhibit the growth of ice crystals to a certain extent. The inhibition of the ice growth depresses the temperature at which already present ice crystals grow, the hysteresis freezing point (T_{hf}), without changing the melting point (T_m) that is predicted by Raoult´s law (the colligative freezing point depression). This separation of the T_{hf} and the T_m is termed thermal hysteresis (TH) or antifreeze activity. It is still debated how AFPs inhibit ice crystal growth; however, the general consensus is that the AFPs recognize and bind to various ice surface planes. Ice growth is restricted to the regions between the adsorbed AFPs causing an increase in local curvature which makes it less favorable for water molecules to join the ice crystal eventually leading to an arrest in its growth [24,30]. The morphology of the ice crystals usually changes to bipyramidal when fish AFPs are absorbed at the ice crystal's surface [9].

Type III AFPs have so far been found in fish belonging to the Zoarcoidei suborder (two Antarctic and five Northern hemisphere species). Type III AFPs are divided into two groups designated SP and QAE after their ability to bind to the ion-exchange matrices SP- and QAE-sepharose, respectively. The two groups share ~50% sequence identity, while within groups the sequence identity is ~90% for the SP group and ~75% for the QAE group. An alignment

of representative type III AFP sequences is shown in Figure 1. Several reports have shown that the QAE isoforms are more active in terms of TH compared to SPs, which are inactive in this respect. A QAE subgroup (QAE2) is also impaired in terms of antifreeze activity. However, SPs, as QAEs, induce the characteristic bipyramidal ice crystal morphology [2,6]. The role of the SPs is still unknown, but *in vitro* the QAE1s and SPs from *Zoarces elongatus* have been shown to co-operate and thereby increase the TH activity to the levels of TH found *in vivo* [21].

The AFPs investigated in this study originate from *Zoarces viviparus* caught in Roskilde fjord. Previous studies have shown by sequence analysis that the AFPs from *Z. viviparus* belong to type III [1,27]. NMR studies of one of them, ZvAFP13, have shown secondary structure elements similar to other type III AFPs [1].

Here we report the expression, purification and X-ray crystal structures for two type III AFPs from *Z. viviparus*, ZvAFP13 representing the QAE1 and ZvAFP6 representing the SP isoform classes, respectively.

2. Materials and methods

Unless otherwise stated, general laboratory chemicals were from Sigma-Aldrich, vectors and strains from Novagen, and enzymes for molecular biology from Fermentas.

Genes, *cloning and expression:* cDNA had been reverse transcribed from mRNA encoding for ZvAFP6 and ZvAFP13 that was isolated from *Z. viviparus*, ligated into pGEM-T Easy vector (Promega) and transformed into JM109 *Escherichia coli* cells (Promega). JM109 *E. coli* cells (Promega) with pGEM-T Easy vector (Promega) carrying the genes encoding for ZvAFP6 (KC622345) and ZvAFP13 (ABN42205) were amplified from the vector by PCR. The mature genes were ligated with T4 DNA ligase into the pET-26b vector after digestion with *NdeI* and *XhoI*. After transformation into the *E. coli* BL21 (DE3), cells were grown at

28°C in LB medium supplemented with 50 µg/ml Kanamycin until cell growth reached OD_{600} 0.7-0.8. To induce expression, 0.5 mM isopropyl thio-β-d-galactoside was added to the LB medium, and the cultures were grown at 28°C for further 16-18 hours. The cells were then pelleted (5000g for 20 min at 4°C), resuspendend in 1/10 volume of 50 mM sodium acetate at pH 8 and lysed by sonication.

Purification: the pH of the supernatant obtained after sonication was adjusted to 4 using 99% acetic acid in order to precipitate most of the non AFPs. The samples were centrifuged (12000g for 20 min at 4°C) and the supernatant applied to a 5 ml HiTrap SP HP cation-exchange column (GE Healthcare) at a flow rate of 0.5 ml/min with a linear NaCl gradient (0–1 M) in 50 mM NaOAc buffer pH 4. The peak fractions were checked for TH and bipyrimidal ice crystal formation. The fractions containing the AFP were pooled and stored at -20°C. The purity was checked on 15% SDS/PAGE gels. The pooled fractions were concentrated using Amicon Ultra 15 centrifugal filter devices with a molecular cut off at 3 kDa (Millipore). The concentration of the protein samples was measured by the BCA Protein Assay Kit (Thermo Fischer Scientific).

Activity: TH was determined as described in Nishimiya et al. [21] and Ramløv [23] using a Nanoliter Osmometer (Otago Osmometers). A cooling rate of 1°C pr. min was used and an annealing time of 1 minute. The ice crystals were as small as possible while still being visible under the microscope.

Native MW estimation: Gel filtration was carried out at 4°C in a 50 mM NaOAc buffer at pH 4.0 containing 0.3 M NaCl using a Superdex 75 column (10/300 GL) and the following proteins as MW standards: aldolase (158 kDa), ovalbumin (43 kDa), carbonic anhydrase (29 kDa) and ribonuclease A (13.7 kDa). Detection of ZvAFP6 was carried out at A_{214} due to the low abundance of aromatics.

For native PAGE 12% gels were used. The gels were run at RT at 150 V for 1.5 h (XCell SureLock© Mini-Cell system; Invitrogen) in 30 mM MES, 30mM histidine, pH 6.1 and with reversed cathode and anode. Ribonuclease A was used as standard.

Crystallization: Initial screenings were setup at RT with an Oryx 8 crystallization robot (Douglas Instruments) in MRC 2 sitting drop plates (Douglas Instruments). Initial conditions were optimized in hanging drops in 24 well VDX plates (Hampton Research) with a drop volume of 4 µl and a reservoir volume of 1 ml. ZvAFP13 crystals grew in 2.5 M $(NH_4)_2SO_4$, 0.1 M citric acid, pH 4.5 with a protein stock concentration of 2mg/ml. ZvAFP6 crystals grew in similar conditions; however, the pH of the citric acid was 4.0 and the protein concentration was 10 mg/ml.

Data collection and processing: A ZvAFP13 and a ZvAFP6 crystal were flash frozen in liquid nitrogen and X-ray data were collected at beamline 911-2 at Maxlab, Lund, Sweden at 100 K with a maximum resolution of 1.45 Å for ZvAFP13 and 1.2 Å for ZvAFP6. Data were processed using XDS [15]. For ZvAFP13 the space group was determined to be $P2_12_12_1$ with 1 molecule in the asymmetric unit. For ZvAFP6 the space group was determined to be $C222_1$ with 2 molecules in the asymmetric unit. Data collection statistics are shown in Table 1.

Structure determination and refinement: the structures of ZvAFP6 and ZvAFP13 were determined by the molecular replacement method with PDB ID 1OPS and 4MSI respectively as search models using Molrep [28]. Cycles of refinement using Refmac5 [20] were alternated with cycles of manual model building in Coot [8]. In the last rounds of refinements the structures were refined anisotropically. The final structures were evaluated with several validation tools including Molprobity [3]. Refinement statistics are in Table 1.

Bioinformatics: For the sequence analysis the type III AFPs sequences deposited at the National Center for Biotechnology Information (NCBI), U.S. National Library of Medicine (http://www.ncbi.nlm.nih.gov/genbank/) were retrieved and aligned using the program MAFFT [16]. The alignments were visualized using BOXSHADE (http://www.ch.embnet.org/software/BOX_form.html). Pymol was used to visualize 3D-structures (Schrödinger), while the PISA server was used to analyze the interfaces [18].

3. Results

Purification: The main purification step in the final procedure was a pH precipitation. The ion-exchange step originally carried out after the pH precipitation actually decreases the purity of ZvAFP13 with respect to higher MW contaminants; therefore this step was later omitted. Furthermore, difficulties were encountered in concentrating the fractions from the ion-exchange step, while the protein could be brought without difficulty to the concentrations necessary for crystallization by concentrating the supernatant from the pH precipitation step.

Activity: Both isoforms induced the previously observed bipyramidal ice crystal morphology. The QAE1 isoform ZvAFP13 had a TH of 0.38±0.03ºC at a concentration of 1 mg/ml and of 0.96±0.01ºC at a concentration of 5 mg/ml. This activity is comparable or higher than the activity reported for other QAE1 isoforms produced recombinantly, as for example in [21] or purified from fish [29]. The SP isoform ZvAFP6 was completely inactive on its own up to a concentration of 10 mg/ml. However, added to ZvAFP13 with both proteins at a concentration of 1 mg/ml nearly doubled the activity (0.75±0.02ºC).

Crystal structures: Well diffracting crystals were obtained for both ZvAFP6 and ZvAFP13. ZvAFP13 crystallizes isomorphously to many other reported type III AFPs [5,13,17], while ZvAFP6 crystallizes, as the first reported type III AFP, in the space group $C222_1$ with two molecules in the asymmetric unit forming a dimer in the crystal (see *Discussion*).

The crystal structure of ZvAFP13 was determined to a 1.45Å resolution. The Cα rmsd with the MR model (PDB ID 4MSI) was 0.384 Å over 52 residues aligned. The structure of the SP isoform, ZvAFP6, was determined to 1.2 Å resolution, representing the first high resolution structure of a SP isoform. The Cα rmsd with the MR model (PDB ID 1OPS) was 0.295 Å for the A chain of ZvAFP6 and 0.268 Å for the B chain, after omitting the two last C-terminal residues of the A chain which are clearly in a different conformation and are not modeled in the B chain. The fold of ZvAFP13 and ZvAFP6 (Figure 2a) is very similar to all other type III AFPs and comprises a compact, globular, single domain.

Overall the electron density is well defined for both proteins, except for the termini. In ZvAFP13, the first three N-terminal residues (M0, N1 and Q2) and the last C-terminal residue modeled (P65) have poor electron density. Alternate conformations are noted in Table 1. All other side chains had excellent electron density showing a single conformation. In ZvAFP6 the N-terminal M could not be modeled, either due to disorder or protease activity found in *E. coli* [19]. Disorder was also observed at the C-terminus, where P65 and Y63 are the last modeled residues for chains A and B respectively, with poor density for the two last residues modeled. In chain B only the side chain density is less defined for the stretch K25-S30. E36 (both chains) and M56A show poor side chain density. Alternate conformations are given in Table 1. P29 is a *cis*-proline in both structures. Additional refinement and geometrical quality information are in Table 1. Final R-factors/R-frees were 13.4%/17.6% for ZvAFP13 and 17.9%/19.5% for ZvAFP6 respectively after anisotropic refinement.

The rmsd for Cα atoms between ZvAFP6 (chain A) and ZvAFP13 was 0.63 Å. Between the A and B chain of ZvAFP6 it was 0.49 Å for all atoms and 0.20 for Cα atoms only.

Native oligomeric state of ZvAFP6: in order to see if the dimeric state of ZvAFP6 in the crystals is also present in solution, gel filtration was carried out. Comparison with standards

shows a MW of around 11 kDa most consistent with a dimer for the most prominent peak (Figure 3A). Native PAGE cannot be run under standard conditions for ZvAFP6 because of its high pI, however by reversing the current it can be electrophoresed at pH 6.1. ZvAFP6 runs close to a ribonuclease A standard, which has approximately the same pI (9.5 vs 9.3 as calculated for ZvAFP6) and double the MW (13.7 kDa) of a ZvAFP6 monomer (Figure 3B). Similar experiments carried out for ZvAFP13 were not conclusive and the MW in solution could not be clearly established.

4. Discussion

Expression and purification: A modification of the protocol by Nishimiya *et al*. [21] for expression of soluble type III AFPs in *E. coli* was followed for the *Z. viviparus* AFPs. Since type III AFPs are still active at low pH [4], the pH of the lysate could be lowered to pH 4, where most *E. coli* proteins precipitated, and an almost pure AFP preparation was obtained, which was suitable for structural studies without further purification.

Activity: Nishimiya *et al.* [21] previously showed that SP and QAE1 type III AFPs from *Z. elongatus* act in a cooperative manner. *Z. viviparus* produces both QAE1s and SPs AFPs, and when combined they also act in a cooperative manner.

Structural determinants for QAEs and SPs differences in activities: The hydration layer of type III AFPs has been subject of many investigations [14,25,26] since the original studies showing that at the ice binding site (IBS) of HPLC12 from *M. americanus* the water structure is ice-like [12,31]. Howard et al. [14] found a cluster of four water molecules, one with weaker density that was close to a tetrahedral geometry in the vicinity of T18, which was used to build a model for the ice face. Equivalents of these waters could be identified in both ZvAFP13 and ZvAFP6, though they are not present in the previously published SP structure

(PDB ID 1OPS) [32], so no obvious difference can be seen in the water structure organization near the IBS for QAE1 and SP variants according to the structures presented here.

The involvement of residues Q9, L10, I13, N14, T15, A16, T18, L19, V20, M21, V41 and Q44 at the IBS has been verified by mutational analysis of the QAE1 isoform HPLC12 from *M. americanus* [2,6,13]. Most of these residues are very well conserved in both QAE and SP proteins, with some variation at Q9 (V in QAE2), I13 (sometimes M in SPs), L19 (V in QAE2s and mostly P in SPs), V20 (G in QAE2s and mostly A in SPs), M21 (one exception), V41 (sometimes an I in QAEs). Recently an inactive QAE2 protein (nfeAFP11) was conferred active similar to an active QAE1 variant through triple or quadruple mutations (V9Q/V19L/G20V and V9Q/V19L/G20V/I41V), underlying the importance of these residues [10].

The most consistent differences between QAE1s and SPs are L19, which in SPs is mostly P, and V20, which in SPs is mostly an A. These two residues were shown to be important for the differences between QAE1 and SP in an investigation by Granham et al. [11] who produced the P19L/A20V variant of a SP isoform (nfeAFP6) from *Z. elongatus* improving its ability to slow down the ice crystal growth 30-fold, however without conferring the ability to arrest ice growth completely. Clearly these residues, while important, do not present the full story, as for example the QAE1 isoform AB1 from *Austrolycicthys brachycephalus* is active (1.27 °C at 2.9mM) and contains P19/A20 [4] like the SP isoforms generally do. Another QAE1, AM1 from *Anarhichas minor*, has P19/I20 at this position. P19/A20 is also not fully conserved in SPs: the Uniprot sequence associated with PDB 1OPS has P19/V20, HPLC1 from *M. americanus* has P19/V20, nfeAFP1, 3 and 4 have L19/A20. All QAE2s have V19/G20.

We note that the nature of the residue at position 37 (I in most QAEs and M in many SPs) is correlated with position 19. AB1, the fully active QAE1 protein mentioned above, which unusually has a P at position 19 also has a M at position 37. Am1 that contains P19 has I37 though, but the activity of Am1 is unknown. As exemplified by the superposition of the ZvAFP13 and ZvAFP6 structures (Figure 2D), L19 and I37 are within contact distance (3.8 Å from L CD2 to I CG2) and it maybe that I at this position is necessary to stabilize the V position. Furthermore if residue 37 were a M it could be expected to destabilize V19, as it would result in contacts as short as 2.5 Å, if it were in the same position as in the ZvAFP6 structure. Thus it could be that an I at position 37 is necessary to fully reap the benefits of L at position 19.

K61 is also a residue that has been discussed in the literature. Mutation of K61 to I affects ice growth inhibition activity and the residue is thought to position N14 correctly, while R47 and D58 form a salt bridge stabilizing the loop on which K61 resides [13]. Since SP isoforms usually lack R47 and/or D58 these residues could play a role in the difference from QAEs as suggested in [11]. However we observe that in both molecules of ZvAFP6 and in PDB ID 1OPS, K61 and N14 are positioned as in ZvAFP13 and other QAEs even though the SPs lack the salt bridge forming residues.

Dimerization of ZvAFP6: The most interesting feature in the ZvAFP6 structure is that the protein forms non-covalent dimers in the crystal as detected by analysis with the PISA server [18]. The interface in the dimers covers an area of approximately 500 $Å^2$ solvent accessible surface per monomer (compared to about 3500 $Å^2$ of total accessible surface for each monomer). The dimer is formed by protein molecules related crystallographically by a two fold axis. The observation of dimers formed by two separate polypeptide chains is to our knowledge unprecedented for type III AFPs, and according to the PISA server prediction the interaction observed in the crystal is strong enough to be of biological relevance in solution.

Gel filtration and native PAGE analysis further supported the formation of dimers in solution for ZvAFP6. Since these techniques are affected by the molecular shape, the shape of the ZvAFP6 dimer observed in the crystal was compared to the crystal structure of bovine ribonuclease A (PDB code 5RSA). Both molecules had slightly elongated shapes. Ribonuclease A has dimensions of about 38 Å in the longest dimension and 20-25 Å in the shortest dimensions (excluding a small 2 residues N-terminal protrusion). The dimer of ZvAFP6 formed in the crystal has also a longer dimension of about 38-39 Å and shorter dimensions around 23-25 Å. Thus it seems reasonable to assume that the results of gel filtration and the native PAGE are reliable.

It is interesting to note that ZvAFP13 is crystallized under similar high sulphate conditions, but does not show dimerization in the crystals; unfortunately, determination of the MW in solution was not conclusive. Two of the residues discussed up to now and which tend to be different in SPs and QAEs, P19 and M37, are very important in dimerization (Figure 2C). F34, fully conserved among the SPs and not found in any of the QAEs, seems also to be essential in forming the interface (Figure 2C).

In the only other available SP crystal structure (PDB ID 1OPS), dimers are not formed. This is hard to rationalize in terms of the few residues that are different between ZvAFP6 and 1OPS at the interface, but may be due to differences in the crystallization conditions for 1OPS, perhaps destabilizing dimerization.

Dimers as observed in the ZvAFP6 crystals could affect ice binding (either favourably or unfavourably), since when the IBS in one of the monomers is bound, the N- and C-terminal tail of the other monomer in the dimer as well as loop 26-35 would protrude towards the ice face. While the biological relevance of dimerization is at this moment in time highly speculative, the demonstration of dimers both in the crystal and in solution for the SP type

ZvAFP6 opens a new dimension for research in the structure-function relationships of AFP type III.

5. Acknowledgments

Dorthe Boelskifte (University of Copenhagen) for technical assistance, the staff at MAXLAB for help with data collection, DANSCATT for travel support, and Thomas F. Sørensen for the genes.

6. References

[1] C.N. Albers, M. Bjorn-Mortensen, P.F. Hansen, H. Ramløv, T.F. Sorensen, Purification and structural analysis of a type III antifreeze protein from the European eelpout *Zoarces viviparus*, CryoLett. 28 (2007) 51-60.

[2] J. Baardsnes, P.L. Davies, Contribution of hydrophobic residues to ice binding by fish type III antifreeze protein. Biochimi. Biophys. Acta 1601 (2002) 49-54.

[3] V.B. Chen, B. Arendall III, J.J. Headd, D.A. Keedy, R.M. Immormino, G.J. Kapral, L.W. Murray, J.S. Richardson, D.C. Richardson, MolProbity: all-atom structure validation for macromolecular crystallography, Acta Cryst. D66 (2010) 12-21.

[4] C.-H.C. Cheng, , A.L. DeVries, Structures of antifreeze peptides from the Antarctic eel pout, *Austrolycicthys brachycephalus*, Biochim. Biophys. Acta 997 (1989) 55-64.

[5] C.I. DeLuca, P.L. Davies, Q. Ye, Z. Jia, The effects of steric mutations on the structure of type III antifreeze protein and its interaction with ice, *J. Mol. Biol.* 275 (1998) 515-525.

[6] C.I. DeLuca, H. Chao, F.D. Sönnichsen, B.D. Sykes, P.L. Davies, Effect of type III antifreeze protein dilution and mutation on the growth inhibition of ice, Biophys. J. 71 (1996) 2346-2355.

[7] J.G. Duman, Antifreeze and ice nucleator proteins in terrestrial arthropods, Annu. Rev. Physiol. 63 (2001) 327-357.

[8] P. Emsley, B. Lohkamp, W.G. Scott, K. Cowtan, Features and development of Coot, Acta Cryst. D53 (2010) 486-501.

[9] G.L. Fletcher, C.L. Hew, P.L. Davies, Antifreeze proteins of teleost fishes, Annu. Rev. Physiol. 63 (2001) 359-390.

[10] C.P. Garnham, Y. Nishimiya, S. Tsuda, P.L. Davies, Engineering a naturally inactive isoform of type III antifreeze protein into one that stop the growth of ice, FEBS Lett. 586 (2012) 3876-3881.

[11] C.P. Garnham, A. Natarajan, A.J. Middleton, M.J. Kuiper, I. Braslavsky, P.L. Davies, Compound ice-binding site of an antifreeze protein revealed by mutagenesis and fluorescent tagging, Biochemistry 49 (2010) 9063-9071.

[12] K.R. Gallagher, K.A. Sharp, Analysis of thermal hysteresis protein hydration using the random network model, Biophys. Chem. 105 (2003) 195-209.

[13] S.P. Graether, C.I. DeLuca, J. Baardsnes, G.A. Hill, P.L. Davies, Z. Jia, Quantitative and qualitative analysis of type III antifreeze protein structure and function, J. Biol. Chem. 274 (1999) 11842-11847.

[14] E.I. Howard, M.P. Blakeley, M. Haertlein, I. Petit-Haertlein, A. Mitschler, S.J. Fischer, A. Cousido-Siah, A.G. Salvay, A. Popov, C. Muller-Dieckmann, T. Petrova, A. Podjarny, Neutron structure of type-III antifreeze protein allows the reconstruction of AFP-ice interface, J. Mol. Recognit. 24 (2011) 724-732.

[15] W. Kabsch, Automatic processing of rotation diffraction data from crystals of initially unknown symmetry and cell constants, J. Appl. Cryst. 26 (1993) 795-800.

[16] K. Katoh, M.C. Frith, Adding unaligned sequences into an existing alignment using MAFFT and LAST, Bioinformatics 28 (2012) 3144-3146.

[17] T.-P. Ko, H. Robinson, Y.-G. Gao, C.-H.G. Cheng, A.L. DeVries, A.H.-J. Wang, The refined crystal structure of an eel pout type III antifreeze protein RD1 at 0.62-Å resolution

reveals structural microheterogeneity of protein and salvation, Biophys. J. 84 (2003) 1228-1237.

[18] E. Krissinel, K. Henrick, Inference of macromolecular assemblies from crystalline state, J. Mol. Biol. 372 (2007) 774-797.

[19] J.-Y. Li, Y.-M. Cui, L.-L. Chen, M. Gu, J. Li, F.-J. Nan, Q.-Z. Ye, Mutations at the S1 sites of methionine aminopeptidases from *Escherichia coli* and *Homo sapiens* reveal the residues critical for substrate specificity, J. Biol. Chem. 279 (2004) 21128-21134.

[20] G.N. Murshudov, A.A. Vagin, E.J. Dodson, Refinement of macromolecular structures by the maximum-likelihood method, Acta Cryst. D53 (1997) 240-255.

[21] Y. Nishimiya, R. Sato, M. Takamichi, A, Miura, S. Tsuda, Co-operative effect of the isoforms of type III antifreeze protein expressed in Notched-fin eelpout, *Zoarces elongatus* Kner, FEBS J. 272 (2005) 482-492.

[22] H. Ramlov, Aspects of natural cold tolerance in ecothermic animals, Human reproduction 15 (2000) 26-46.

[23] H. Ramløv, Measuring antifreeze activity. In Graether, S.P (Ed.), Biochemistry and Function of Antifreeze Proteins, Nova Science Publishers Inc., New York, 2010, pp. 7-42.

[24] J.A. Raymond, A.L. DeVries, Adsorption inhibition as a mechanism of freezing resistance in polar fishes, Proc. Natl. Acad. Sci. U. S. A. 74 (1977) 2589-2593.

[25] A.B. Siemer, K.-Y. Huamg, A.E. McDermott, Protein-ice interaction of and antifreeze protein observed with solid-state NMR, PNAS 107 (2010) 17580-17585.

[26] N. Smolin, V. Dagett, Formation of ice-like water structure on the surface of an antifreeze protein, J. Phys. Chem. B 112 (2008) 6193-6202.

[27] T.F. Sorensen, C.H. Cheng, H. Ramlov, Isolation and some characterization of antifreeze protein from European eelpout *Zoarces viviparus*, CryoLett. 27 (2006) 387-399.

[28] A. Vagin, A. Teplyakov, MOLREP: an automated program for molecular replacement, J. Appl. Cryst. 30 (1997) 1022-1025.

[29] X. Wang, A.L. DeVries, C.-H.C. Cheng, Antifreeze peptide heterogeneity in an Antarctic eel pout includes an unusually large major variant comprised of two 7 kDa type III AFPs linked in tandem, Biochim. Biophys. Acta 1247, 163-172.

[30] P.W. Wilson, Explaining thermal hysteresis by the Kelvin effect, CryoLett. 14 (1993) 31-36

[31] C. Yang, K.A. Sharp, The mechanism of the type III antifreeze protein action: a computational study, Biophys. Chem. 109 (2004) 137-148.

[32] D.S. Yang, W.C. Hon, S. Bubanko, Y. Xue, J. Seetharaman, C.L. Hew, F. Sicheri, Identification of the ice-binding surface on a type III antifreeze protein with a "flatness function" algorithm, Biophys. J. 74 (1998) 2142-2151.

7. Figures and tables

Table1: Data collection and refinement statistics.

Figure 1: Sequence alignment of type III antifreeze proteins mentioned in the discussion. Asterisks indicate ice binding residues, residues with grey background are the mutations that are mentioned in text, and residues with black background are the ones that are important in dimerization of ZvAFP6.

Figure 2a-d: A) Superimposition of ZvAFP6 (orange), ZvAFP13 (green), RD1 from *Lycodichthys dearborni* (pink) (PDB ID: 1UCS), HPLC12 from *Zoarces americanus* (yellow) (PDB ID: 4MSI), and HPLC3 from *Zoarces americanus* (blue) (PDB ID: 1OPS). B) superimposition of presumed ice binding residues of ZvAFP6 (orange) and ZvAFP13 (green). C) The interface between ZvAFP chain a (orange) and chain b (purple). F34 and M37 are presented as sticks and the ice binding site residues are presented as spheres, with carbon atoms colored as the rest of the monomer, sulfur in yellow, oxygen in red and nitrogen in blue. D) Overlay of residues 19 and 37 from ZvAFP6 (orange) and ZvAFP13 (green).

Figure 3: Native oligomeric state of ZvAFP6 in solution. A) Gel filtration trace, with Ribonuclease A in black (13.7 KDa) and ZvAFP6 in grey. The major peak corresponds to a size of circa 11 kDa Inset: SDS-PAGE of loaded ZvAFP6 sample (S) and selected fractions (F1-F3, 1 mL fractions between 12-15 mL elution volume). M are the MW markers (97 to 14 kDa)) B: Native PAGE of ZvAFP6 and Ribonuclease A.

Table1: Data collection and refinement statistics.

Protein	**ZvAFP13**	**ZvAFP6**
PDB code	4UR4	4UR6
Space group	$P2_12_12_1$	$C222_1$
Unit cell dimensions (a, b, c in Å)	32.26; 39.69; 44.22	75.57; 108.17; 38.25
Resolution	1.45-29.54 (1.45-1.49)	1.20-30.0 (1.20-1.23)
Completeness (%)	98.0 (92.5)	98.5 (94.9)
Redundancy	4.4 (3.4)	6.2 (5.0)
R_{rim} (%)	4.0 (31.1)	3.1 (42.7)
No. of reflections	45146 (2448)	300182 (17280)
No. of unique reflection	10321 (715)	48601 (3431)
I/σ_I	24.2 (4.7)	25.2 (5.2)
R_{work}	0.134	0.179
R_{free}	0.176	0.195
Rmsd bonds (Å)	0.015	0.018
Rmsd angles (º)	1.864	1.819
Modelled solvent and other components	90 water molecules	205 water molecules 2 sulphate ions
Residues in alternate conformation	Q2, Q9, L10, E25, T28, M30, P38, L40, S42, M43, L55 and Y63	L10(A), I13(B), S30(A/B), M37(A/B), Q39(A), L55(A/B), D58(A).
Ramachandran plot		

(Molprobity)		
Residues in favored regions (%)	98.4	100.0
Residues in allowed regions (%)	100.0	100.0
Outliers	None	None

Figure 1

```
                          1                   20                  40                  60
HPLC1 (SP) (P19608)       -SQSVVATQLIPMNTALTPVMMEGKVTNPIGIPFAEMSQIVGKQVNTPVAKGQTIMPNMVKTYAA--
1OPS (SP) (1OPS_A)        -SQSVVATQLIPMNTALTPAMMEGKVTNPIGIPFAEMSQLVGKQVNTPVAKGQTLMPNMVKTYAA--
nfeAFP6 (SP) (BAD95781)   -GESVVATQLIPINTALTPAMMEGKVTNPSGIPFAEMSQIVGKQVNTPVAKGQTLMPGMVKTYVPAK
ZvAFP6 (SP) (KC622345)    -GESVVATQLIPINTALTPAMMAGKVTNPSGIPFAEMSQIVGKQVNTPVAKGQTLMPDMVKTYVPAK
Ab1 (QAE1) (P12100)       -TKSVVASQLIPINTALTPAMMKAKEVSPKGIPAEEMSKIVGMQVNRAVNLDETLMPDMVKTYQ---
ZvAFP13 (QAE1) (ABN42205) NQASVVANQLIPINTALTLVMMRAEVVTPMGIPAVDIPRLVSMQVNRAVPLGTTLMPDMVKGYAPA-
HPLC12 (QAE1) (P19614)    NQASVVANQLIPINTALTLVMMRSEVVTPVGIPAEDIPRLVSMQVNRAVPLGTTLMPDMVKGYPPA-
nfeAFP11 (QAE2) (BAD95786) NQESVVAAVLIPINTALTVGMMTTRVVSPTGIPAEDIPRLISMQVNQVVPMGTTLMPDMVKGYAPA-
Am1 (QAE1) (ABA41378)     HQASIVANQLIPINTALTPIMTKAQVVTPLGIPAEDIPRIIGMQVNRAVALGTTLMPDMVKGYPPN-
                                  **  **** ****                  *  *
```

Figure 2

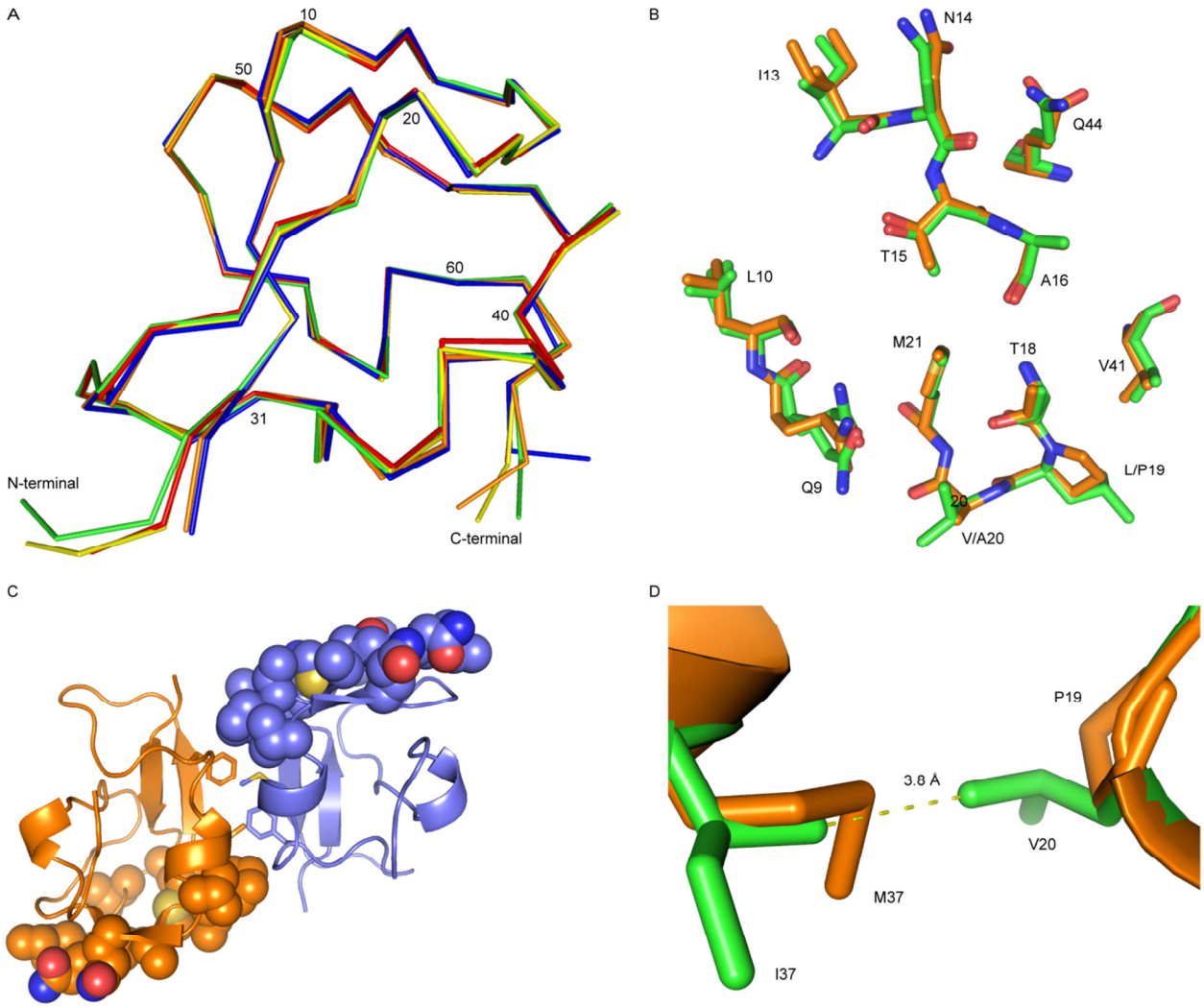

Figure 3

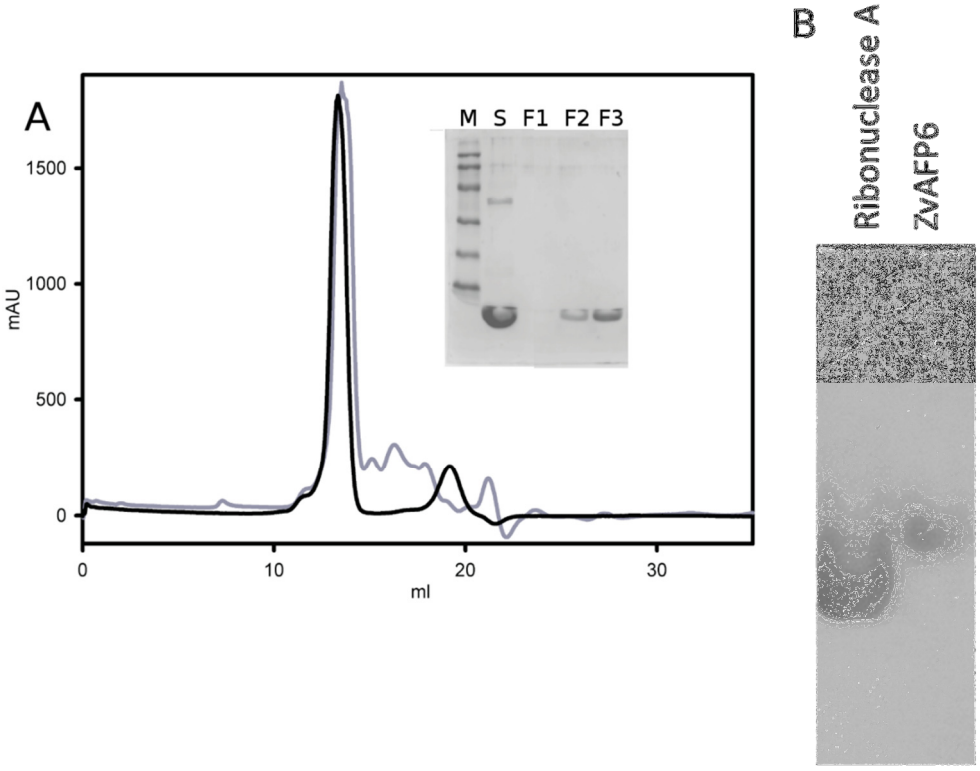
A
M S F1 F2 F3
1500
1000
500
0
mAU
0
10
20
30
ml
B
Ribonuclease A
ZvAFP6